POLITECNICO DI TORINO
Repository ISTITUZIONALE

In situ generation of silver nanoparticles in PVDF for the development of resistive switching devices

Original
In situ generation of silver nanoparticles in PVDF for the development of resistive switching devices / Chiappone, A., Gillono, M., Castellino, M., Bejtka, K., Rajan, K., Roppolo, I., Perrone, D., Bocchini, S., Ricciardi, C., Pirri, C.F., Chiolerio, A.. - In: APPLIED SURFACE SCIENCE. - ISSN 0169-4332. - 455:(2018), pp. 418-424. [10.1016/j.apsusc.2018.06.001]

Availability:
This version is available at: 11583/2709478 since: 2019-09-17T11:29:34Z

Publisher:
Elsevier

Published
DOI:10.1016/j.apsusc.2018.06.001

Terms of use:

This article is made available under terms and conditions as specified in the corresponding bibliographic description in the repository

Publisher copyright

(Article begins on next page)

26 November 2026

In situ generation of silver nanoparticles in PVDF for the development of resistive switching devices

A. Chiappone*[1], M. Gillono[1], M. Castellino[2], K. Bejtka[1], K. Rajan[1,2], I. Roppolo[1,2], D. Perrone[1], S. Bocchini[1], C. Ricciardi[2], C.F. Pirri[1,2], A. Chiolerio[1]

[1] *Center for Sustainable Future Technologies, Istituto Italiano di Tecnologia, Corso Trento 21, Torino 10129, Italy*

[2] *Department of Applied Science and Technology, Politecnico di Torino, Torino, Corso Duca degli Abruzzi 24, 10129, Italy*

**Corresponding author: annalisa.chiappone@polito.it current address: Department of Applied Science and Technology, Politecnico di Torino, Torino, Corso Duca degli Abruzzi 24, 10129, Italy*

Abstract

It is widely accepted that resistive switching devices (RSDs) are extremely appealing as active components in computer memories and logic gates in electronics, directly enabling neuromorphic functionalities. The aim of this study is to investigate the chemical and electrical properties of a nanocomposite polymer, the active component of the device, in order to characterise its composition and behaviour under electric field. This paper presents the morphological and chemical characterization of an in-situ generated silver – Polyvinylidene fluoride-hexafluoropropylene PVDF-HFP nanocomposite (NC) material. A silver salt is added as precursor to the polymer solution and then, after a film casting step, the nanoparticles generation and growth processes are carried out by way of UV irradiation; the growth and the distribution of in-situ generated silver nanoparticles (NPs) in the polymer matrix are described. The devices, built on a planar electrode structure, undergo an I/V test to explore their resistance states at different switching voltages. Furthermore, after electrical analysis a remarkable R_{off} / R_{on} ratio and a relatively low switching voltage (3 V) are achieved, demonstrating the suitability of the developed material for the next generation of soft, wearable, RSDs.

Keywords: silver nanocomposite; PVDF; in-situ generation; resistive switching

1. Introduction

The existence of memristors was firstly hypothesized in the early ‘70s by Leon Chua who described, through a mathematical equation, a device that can provide a relationship between flux and charge as a nonlinear resistor can do between voltage and current.[1]

The ideal memristor, in a broader sense known as resistive switching device (RSD), is typically a stacked structure in which the resistance varies when a certain positive current flows through it and remains frozen until a 'reset' negative current flows when a negative voltage is applied.[2] Thus the device will be characterized by its R_{on} and R_{off} resistance states.[3]
The intriguing ability of freezing two resistance states makes RSDs suitable for computer memories and useful as logic gates also in neuromorphic computing, mainly because of the innate capability of showing plasticity, or programmable states on the basis of stimulus strength or stimuli timing.[4-8] RSDs nowadays studied and reported in literature are fabricated involving three different families of materials. In the majority of published works, inorganic RSDs are reported, probably because of their highly controllable structure, their easy deposition in the form of thin films and their good compatibility with complementary metal oxide semiconductor (CMOS) processes. [9, 10] In this typology of devices the active layer is typically composed of oxides (e.g. TiO_2[10], Gd_2O_3[11], SiO_2[8], etc.) sandwiched between two metal electrodes and the resistive switching mechanism is more commonly attributed to the drift of oxygen vacancies with an applied electric field.[11-13] For what concerns organic RSDs, they are rather different systems and their functioning mechanism is still under debate.[14] Nevertheless, polymer materials are seen as promising candidates for the development of high performing RSDs thanks to their low cost, easy processability, mechanical flexibility and easy tuning of the electronic performance through innovative molecular design. [15-18] The third class of resistive switching devices is based on nanocomposite (NC) materials; in this case an insulating polymer is used as matrix for active fillers or nanoparticles (NPs).[19-22]

The RSDs that fully respond to the requirements of memristors are usually used for creating large crossbar arrays for various applications, and in this case sneak path current becomes a major issue. Selector devices, that can be seen as another kind of RSDs, play an important role in the mitigation of this unwanted current. Nowadays many research teams are also working on mitigating this sneakpath current issue by using selector devices[23] without compromising the scalability of memristors. The key requirement for a selector device is that it should have a large On/Off ratio, a steep turn on slope, high current density, fast turn On and Off .[24] Several kinds of selectors have been recently presented. [24-27] Silver-based polymer NCs RSD reported in literature seem to present some of the required features for selectors.[22, 28, 29]

The careful study of the material can help in controlling and understanding its behaviour when submitted to electrical stresses. Nanometric materials present amazing electronic properties which enable their use for the development of innovative RSDs and, in particular, selectors. Furthermore, polymer NCs usually require much easier production processes with respect to inorganic structures and give, at the same time, high throughput processing, light-weight and mechanical flexibility.[22]

Furthermore, the typical low operational voltages encourage their use in direct connection with living biological neurons.[30]

Two different approaches can be followed for the production of NC materials: the nanometric fillers can be directly added into the polymer matrix (ex-situ method) or, alternatively, some precursors of the nanophase can be mixed into the polymer matrix and NPs are generated in-situ during the polymerization or through a dedicated post processing (in-situ method).[31-33]

Ex-situ synthesis is commonly more appropriate for large-scale industrial applications than in-situ synthesis even if problems linked to the uniform dispersion and aggregation of NPs must be tackled. On the other hand, the in-situ synthesis approach is simple and effective in preventing particle agglomeration while maintaining a good spatial distribution in the polymer matrix; these advantages of the in-situ NCs result extremely appealing when the application in electronic devices is envisaged.[34]

In this paper in-situ NC materials are studied. Silver salts are added to a solution of Polyvinylidene fluoride-hexafluoropropylene (PVDF-HFP) and the NPs in-situ generation is then UV-induced in spin-coated films. PVDF as well as its copolymer PVDF-HFP can be chosen as polymer matrix for such application being known its high dielectric constant, chemical stability and good mechanical strength; this polymer can act as a quasi-solid medium for metal ions during the photoreduction of the silver salt and during the functioning of the device supporting the ionic movements when an electric field is applied. [35]

UV-VIS and XPS analyses are provided in order to investigate the effective presence of the NPs and their growth in the polymer matrix by photochemical reduction; FESEM analysis are performed in order to directly see the morphology of the NC polymer structure and geometrical distributions are extracted using a numerical algorithm. Electrical characterizations are carried out on chips where the NC material is coated in order to qualify its resistive switching under applied variable voltage.

2. Methodology

2.1 Materials

Poly(vinylidene fluoride-hexafluoropropylene) (PVdF-HFP) KynarSuperflex 2500 (pellets) with 20 wt% of hexafluoropropylene and a density 1.79 g cm^{-3} was purchased from Arkema. Silver nitrate ($AgNO_3$) (99%), dimethylformamide (99.5%) (DMF) were purchased from Sigma Aldrich.

2.2 Sample preparation

The NC polymer acting as resistive switching material was prepared as follow: a solution of PVDF-HFP in DMF (10wt%) was obtained by vigorous mechanical stirring for 15 minutes to obtain the complete dissolution of the polymer in the solvent. Different amounts of $AgNO_3$ (5, 20 and 50 phr, per hundred resin) were then added to the solution and carefully mixed in ultrasound bath for 30 minutes; lower concentrations are not presented since they gave open circuit devices. The obtained formulations were uniformly poured on a silicon chips and spin coated at 1000 rpm for 10 seconds and at 2000 rpm for other 10 seconds. At the end of the process, a uniform and thin (400 to 500 nm) layer was formed on the chip's surface. The chip used in the experiments was composed by a silicon substrate with gold patterns deposited on it.[22] The electrodes were separated by a 10 μm gap filled with the active NC material. In a final step, the chip with the NC polymer deposited on it was individually irradiated with UV light using an ultraviolet lamp with light intensity of 10 mW/cm^2 for one hour. This process was necessary for the reduction of $AgNO_3$ and the formation of the silver NPs. The samples corresponding to the different formulations are referred to as 5 $AgNO_3$, 20 $AgNO_3$ and 50 $AgNO_3$.

2.3 Characterization methods

The UV–Visible spectra were recorded with of a double beam Lambda 40 instrument (Perkin-Elmer). The range of the wavelength between 280 and 800 nm was monitored with a scan step of 1 nm.

The solution of polymer and silver salts was gently deposited and spin coated on a glass slide. After that, the UV-vis spectra were collected at different exposure times of UV radiation.

XPS spectra were obtained using a PHI 5000 Versaprobe Scanning X-ray Photoelectron Spectrometer (monochromatic Al K-α X-ray source with 1486.6 eV energy). The surface chemical composition and Ag NPs distribution in depth were investigated using a spot size of 100 μm in order to collect the photoelectron signal for both the high resolution (HR) and the survey spectra. Different pass energy values were exploited: 187.85 eV for survey spectra and 23.5 eV for HR peaks. All samples were analysed with a combined electron and Ar ion gun neutralizer system in order to reduce the charging effect during the measurements. All core-level peak energies were referred to C1s peak at 284.5 eV and the background contribution in HR scans was subtracted by means of a Shirley function. The software Multipak 9.6 was used to analyse the obtained spectra. A depth profile analysis was also performed, by means of an Ar^+ flux at 2 kV accelerating voltage and (2x2) mm^2 area, in an alternate mode with sputtering cycles of 1 min each.

A morphological analysis of the NC samples was done with Field Emission Scanning Electron Microscopy (FESEM, ZEISS Dual Beam Auriga) after platinum metallization of the surface. The

sample for the cross-section characterization has been prepared with the use of Focused Ion Beam (FIB, Zeiss Dual Beam Auriga) operated at 30kV. Thick platinum protection layer was deposited prior to the sectioning.

Images of the reduced silver NPs were taken and their size distribution was quantified using a Matlab ® routine able to extract geometrical parameters such as equivalent diameter, branching factor, mean distance between particles, orientation, eccentricity.[36]

The electrical characterization was performed on the chips by means of a Keithley 4200-SCS Semiconductor Characterization System, using standard 2-point setup and contacting the samples by tungsten microneedles firmly placed directly on the gold electrodes.

The measurements were performed applying a voltage varying between a positive and a negative value with a scan step of 50 mV and a set current compliance of 10 µA. The applied voltage range was changed for every sample in order to achieve the desirable resistive switch. For each sample 5 cycles of the I/V characteristic were performed. All the electrical characterizations were performed at room temperature.

3. Results and discussion

Before investigating the electrical behaviour of the silver/PVDF NC, the in situ generation of Ag NPs was studied; firstly, the nucleation and growth mechanism was followed by means of UV-vis analyses. The PVDF solutions containing different amounts of silver nitrate (5, 20 and 50 phr) were spin coated and the obtained films were characterized after different UV-exposure times in order to investigate the kinetics of growth of Ag NPs.

In fact, silver ions can undergo reduction from Ag^+ to Ag^0 under UV-irradiation and in presence of an electron donor.[32] Being known from literature that some radicals can be generated at the surface of UV irradiated fluorine based polymers, [37] [38] these can then be used as electron donors in order to reduce the silver ions to metallic silver leading to the formation of Ag NPs embedded in the polymeric matrix through UV exposure.[39] Silver NPs have got a characteristic absorption peak centred at about 450 nm that is linked to the surface plasmonic resonance band; the height of the peak can be linked to the quantity of NPs.[40]

Figure 1 a, b, c show the absorption of the plasmon peak for the different samples (5 $AgNO_3$, 20 $AgNO_3$ and 50 $AgNO_3$) growing in intensity with the increase of UV exposure time, indicating the rising of the nanoparticles concentration. Figure 1,e also reports the maximum height of the peak as a function of irradiation time showing the continuous increase of the height during irradiation.

The evolution of the wavelength corresponding to the maximum of the peak (λ_{max}) is reported in Figure 1d. It is known that even small differences in the peak position (λ_{max}) can be related to the NPs size.[28] Observing the plots, it is possible to notice that increasing the amount of silver precursor the λ_{max} of the plasmon peak increases from about 410 nm for sample 5 $AgNO_3$ to 460 nm for sample 50 $AgNO_3$ (Figure 1,d) indicating the presence of bigger particles in the samples containing higher quantities of silver precursor. λ_{max} also slightly increases for the samples 5 $AgNO_3$ and 20 $AgNO_3$ during irradiation while in sample 50 $AgNO_3$ it is possible to evidence the presence of bigger nanoparticles since the beginning of the irradiation.

The growing peaks also show a broadening with the increase of the irradiation time, which can be related to the increase of the NPs volume fraction.

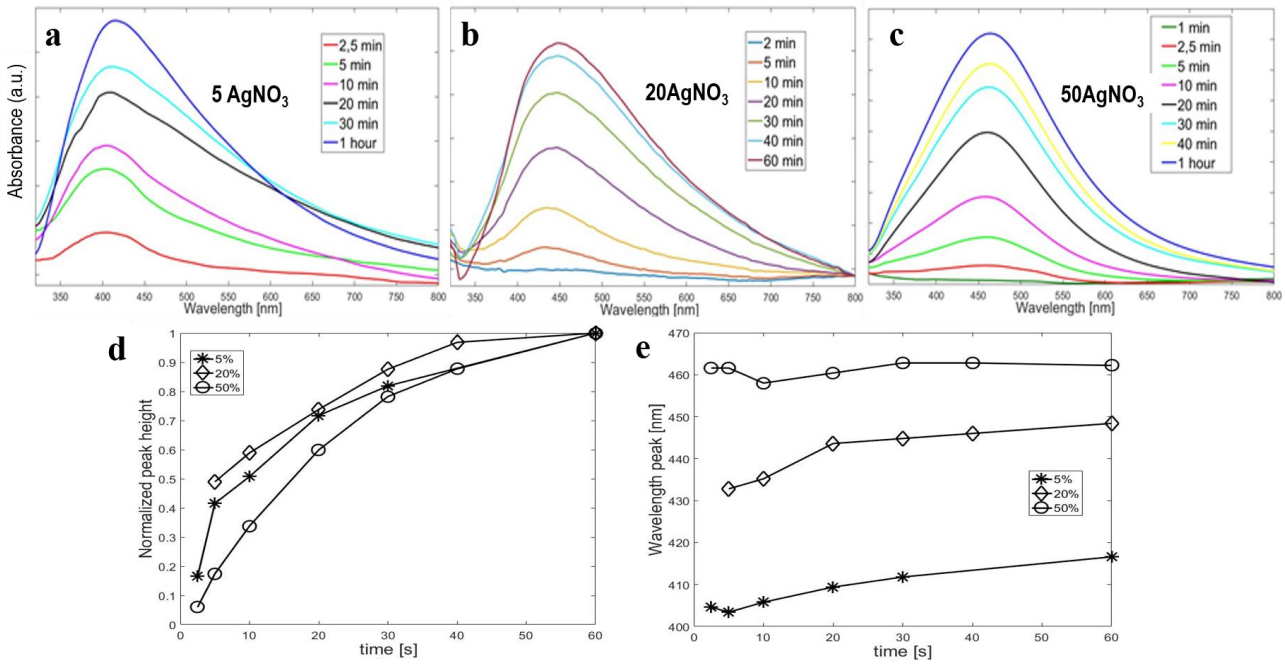

Figure 1 UV-Vis spectra depicting the silver nanoparticles growing kinetic for sample 5AgNO3 (a), 5AgNO3 (b) and 50AgNO3 (c) the normalized peak amplitude (d), and the peak wavelength (e)

FESEM images were collected to observe the surface of the neat polymer and of the samples containing different amounts of silver precursor after 1 hour of irradiation.

Figure 2 reports the collected images; it is visible that the polymeric matrix without the precursor shows smooth and NPs free surface, while the NC matrices show the presence of the Ag NPs. Their number is relatively high and distribution is quite homogeneous. The NPs size and density highly depends on the precursor concentration. For the higher percentages studied an agglomeration of the Ag NPs is also observed.

The samples were also studied in the cross-section view in order to estimate their thickness and NPs distribution. The thickness of the spin coated material was of 400 to 500 nm (Figure S1a) for all the samples. A representative image of the cross-section at higher magnification for the sample 5 $AgNO_3$ is presented in Figure S1b, showing relatively small number of NPs generated in depth in respect to the surface.

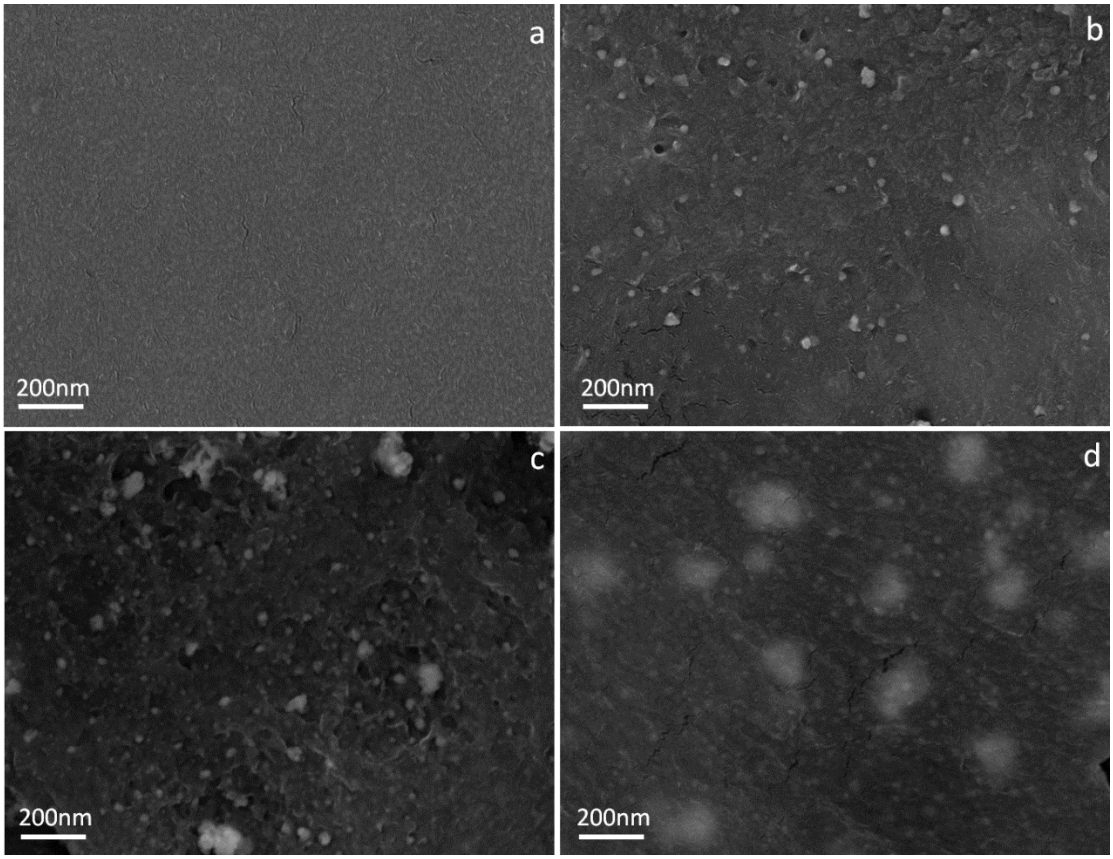

Figure 2 FESEM micrographs showing the top view of NC samples with varying concentration of $AgNO_3$, (a) 0, (b) 5, (c) 20 and (d) 50 phr.

By means of numerical geometrical analysis, we extracted the statistics shown in Figure 3. Sample 5 $AgNO_3$ shows well distributed NPs with a size mainly distributed in the range 5 to 40 nm, counting rare bigger aggregates (Fig. 3a). Sample 20 $AgNO_3$ shows a good NPs distribution of particles having the same small scale distribution, but experiencing a more statistically significant presence of bigger aggregates (up to 170 nm, Fig. 3b). Sample 50 $AgNO_3$ features the smaller NPs with a broader distribution, up to 50 nm, embedded in the polymer matrix, and an even higher amount of aggregates (up to 190nm, Fig. 3c). The very good distribution and high number of NPs observed in the samples containing lower amounts of silver precursor gives high probability for charge carriers to move through the sample and pass the gap between the electrodes. This is confirmed by analyzing the distance between particles, our algorithm outputs similar distributions

with peaks shrinking as the precursor content increases: the median of the distances for sample 5 $AgNO_3$ is 33 nm (Fig. 3d), for sample 20 $AgNO_3$ is 15 nm (Fig. 3e), for sample 50 $AgNO_3$ is 15 nm (Fig. 3f). Furthermore the presence of smaller NPs, not visible by FESEM analysis, can be supposed.[28] Another relevant analysis performed with the aid of the numerical routine evidences the shape and preferential orientation of the NPs in the matrix; the greatest amount of particles are not preferentially oriented. From a purely geometrical point of view, the first moment of the surface of a big number of NPs is non-zero and therefore they have an eccentricity: for sample 5 $AgNO_3$ the median is 0.7 (Fig. 3g), for sample 20 $AgNO_3$ 0.55 (Fig. 3h) and for sample 50 $AgNO_3$ again 0.7 (Fig. 3i). Besides this we see the weight of perfectly spherical NPs changing from marginal (5 $AgNO_3$) to considerable (20 $AgNO_3$) to predominant (50 $AgNO_3$).

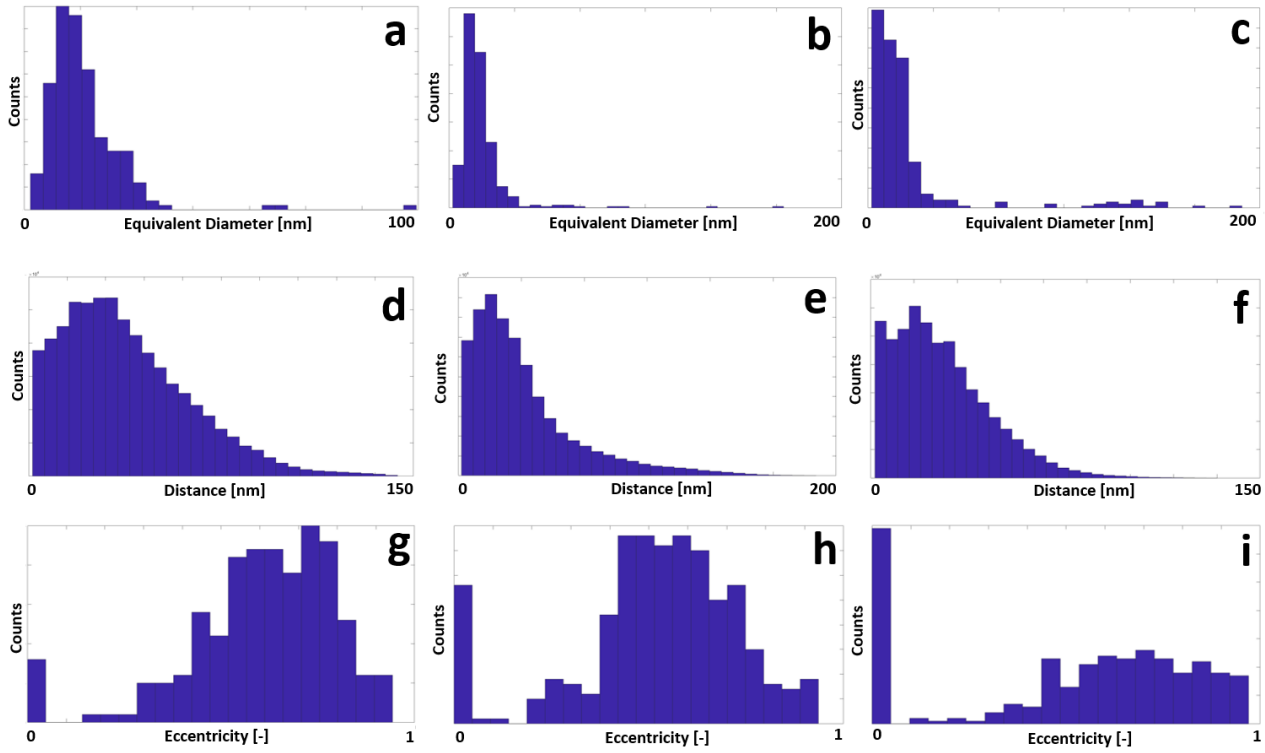

Figure 3 Geometrical statistics extracted from the FESEM images of Figure 2, with varying concentration of $AgNO_3$: 5 (left column), 20 (middle column), and 50 phr (right column), showing their properties: the equivalent diameter (upper row), the inter-particle distance (middle row) and the eccentricity (bottom row).

Spin coated films of the 3 samples were then analysed by XPS in order to check the presence of metallic silver and to obtain more information about the generation of NPs. Figure 4 (upper line) reports the survey spectra of the samples; here the peaks at 284-290 eV and 688 eV correspond to the typical signals of carbon C1s and fluorine F1s respectively that are found in the PVDF matrix. The silver component is detectable from the two characteristic peaks at 368 eV ($Ag3d_{5/2}$) and 374

eV ($Ag3d_{3/2}$) while the band at 532 eV is related to the presence of oxygen O1s that indicates a surface oxidation. From the spectra is also visible that there is no nitrogen deriving from the counter ion NO^{3-} that should have had its peak centred at 400 eV. This was expected according to the literature on the photochemistry of nitrate ions that shows that volatile NO_2 can be released during UV irradiation.[36]

High resolution (HR) measurements have been performed in the C and Ag core peaks region (See SI). The carbon peaks detected on the surface always show the presence of the C-C and C-F bonds (Figure S2). In Figure S3 the Ag3d HR spectrum is reported together with its deconvolution curves, obtained by means of a mixed Gauss–Lorentz curve fitting. Reference values of binding energy for metallic Ag are 368.2 eV and 374.2 eV.[28] Sample 20 $AgNO_3$ shows its peaks at that energy value indicating the presence of relatively big silver particles, while the shifts toward higher binding energy values observed in samples 5 and 50 $AgNO_3$ can be correlated to a different size of the NPs on the surface.[30] This observation can match with the collected FESEM images; in fact while sample 20 $AgNO_3$ presents some aggregate visible on the surface of the sample, sample 5 $AgNO_3$ presents thinnest particles and sample 50 $AgNO_3$, instead, shows bigger aggregates that seems below a first polymer layer (Figure 2, size distributions in Figure 3).

To better investigate the structure of the produced nanocomposites, depth profile analysis was performed on all the samples. An Ar^+ source with a 2 kV acceleration voltage and a (2 × 2) mm^2 square area was used, alternating the acquisition mode with 1 min of sputtering cycle for a total amount of 60 cycles; it can be assumed that the sample has been analysed in a depth of about 300-400 nm. The high resolution peaks related to C_{1s} collected during depth profile are reported in the supporting informations (Figure S4); as visible, the CF_2 peak (290 eV) is present only at the surface while in the inner part of the samples fluorine is almost no more detected, this is due to the hydrophobic nature of fluorine. Aiming to observe the growth and distribution of the silver nanoparticles, the Ag_{3d} peak has also been analysed (Figure 4, second row): the three samples present different behaviour.

Sample 5 $AgNO_3$ shows a migration of the silver nanoparticles at the surface with a visible enrichment in the first layers, which is in line with the FESEM observation. The phenomenon of the silver NPs migration toward the surface of the polymer matrix was already observed in different cases of UV-induced in situ generation.[28, 40] Sample 20 $AgNO_3$ presents an enrichment in the top layer, a lower amount of silver detected in the layers directly below the surface and then again an increase of the silver peak height towards the core of the sample, creating a depletion volume just underneath the surface. Differently, sample 50 $AgNO_3$ present a poorer surface concentration and then an almost constant amount of silver is detected in the thickness of the sample. Those

phenomena are of difficult explanation: it could be supposed that the higher amount of silver precursors dispersed in the polymeric matrix, the higher is the light absorption at the surface, inhibiting a deeper penetration of the radiation. This could disable the grow-disruption-rebuilding mechanism of silver NPs that usually occurs under light radiation and favours NPs' surface enrichment[41, 42]. This could explain both the depletion zone evidenced in 20 $AgNO_3$ sample and the homogeneous distribution in 50 $AgNO_3$ sample. On the other hand, since those migration phenomena are even thermally controlled, effects related to the film thickness and to the substrate could be taken into consideration[43]. More experiments are necessary to better elucidate this point. The trend observed for this sample matches with the FESEM observation where bigger particles are visible below the first polymeric layer.

Observing the NPs morphology and distribution, the sample containing the lower amount of silver precursor seems more promising for its use as switching device without running across short circuiting phenomena.

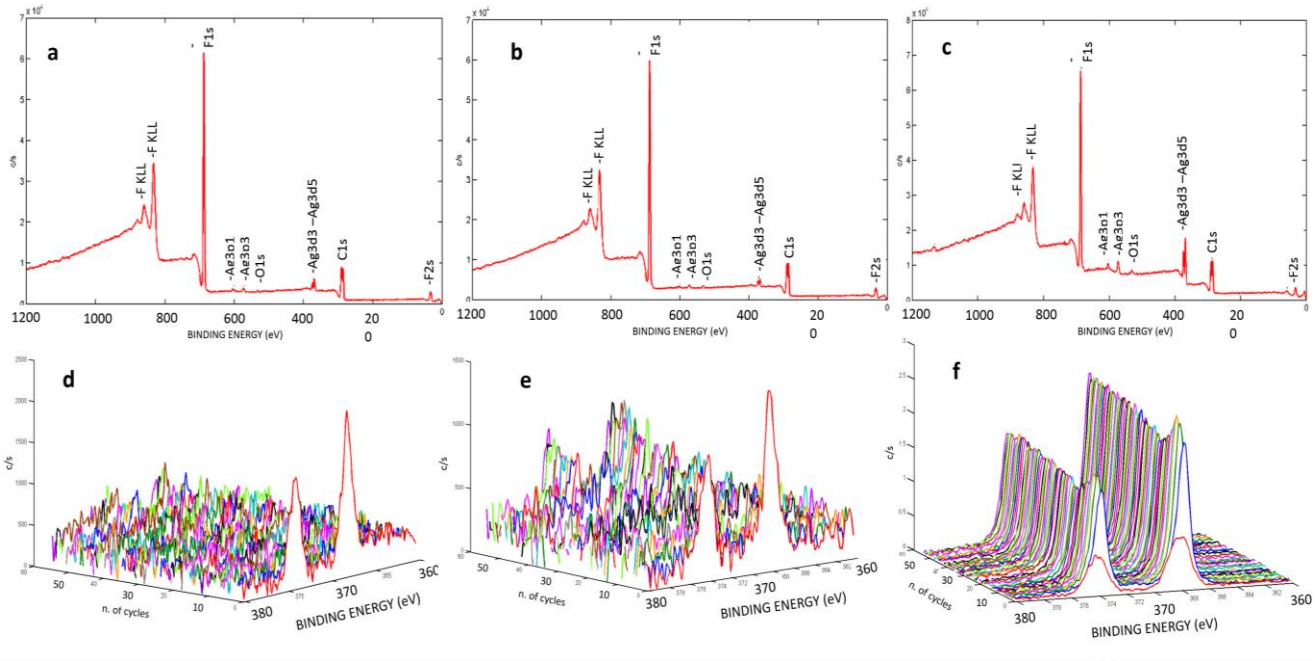

Figure 4 XPS survey spectra (upper row) for the 5 (a), 20 (b) and 50 (c) $AgNO_3$ samples. Ag3d (lower row) HR spectra collected during the depth profile acquisition for all the the 5 (d), 20 (e) and 50 (f) $AgNO_3$ samples.

The behaviour of the studied NCs as resistive switching (RS) was then investigated. RS consists in the sudden switching between two resistance states due to the application of an electric stress, as reported in literature [17,19] . In metal−polymer NCs the mechanism is driven by the formation of conductive metallic bridges between the electrodes, while the electrical bistability is explained by a redox and dissolution of silver ions back into the matrix[17]. For this reason the control over the NPs

size and distribution can result extremely important for the understanding of the device. The three samples were tested on a planar chip made of two symmetrical gold electrodes (Figure 5a) to check their behaviour but, as expected, the use of high amounts of silver precursor lead to short circuiting effects and only sample 5 $AgNO_3$ gave promising results. Therefore only the characterization of this sample will be discussed.

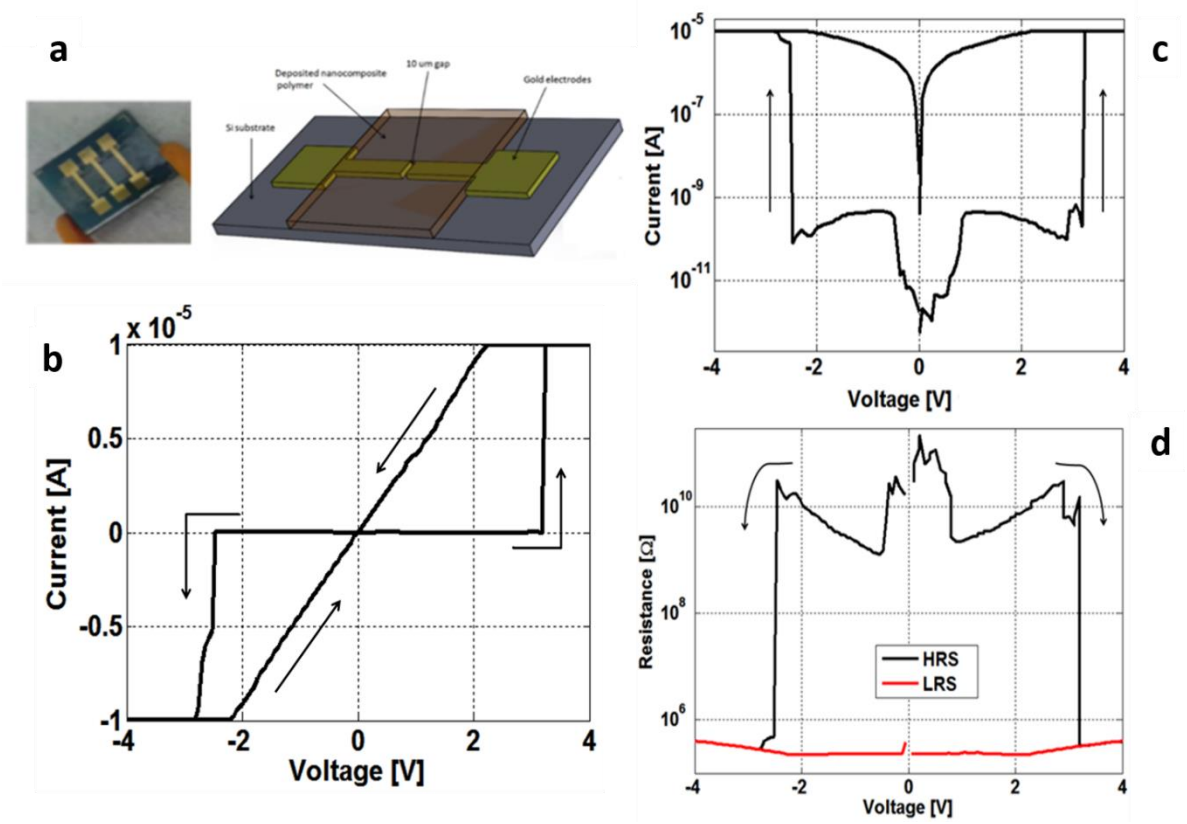

Figure 5 Representation of the planar chip structure (a), I-V measurements, fifth I-V cycle of the RSD (b), cyclic logarithmic IV measurement performed on the RSD with a compliance of 10 μA (c), resistance variation during the voltage sweep (d)

Cyclic I-V measurements between +4 and -4 V were performed in order to understand the switching behaviour of the built device. Figure 5b illustrates the fifth I-V cycle of the RSD, reported as representative, with a set voltage of 3.2 V corresponding to an electric field of 3.2 kV/cm. In all the performed tests, the first cycle always needs the application of a higher initial electroforming voltage, approaching an electric field of 4 kV/cm; in this way the pristine device which was in a high resistance state (HRS) passed to its low resistance state (LRS). It can be supposed that by the application of this field, the silver NPs and ions move to form a filamentary path bridging the two gold electrodes, as already described in literature.[22] Once the initial electroforming was performed, the following set process took place at a lower voltage, as shown in figure 5b. The device behaves

as a random access memory in which the information was lost when the power is turned off; such a behaviour can result interesting for selector devices.

Figure 5c reports the cyclic logarithmic IV measurement performed on the RSD with a compliance of 10 μA showing an instantaneous increase of the current when the switching voltage is applied. Figure 5d shows the resistance variation during the voltage sweep. The switch from HRS to LRS, for both positive and negative cycles, is displayed with a HRS/LRS ratio of about 5 orders of magnitude which can result promising for the possible application of this NC as active material for selectors.

4. Conclusion

In situ generated silver-polymer NCs have been studied and their resisting switching behaviour has been investigated. Silver NPs were generated inside a PVDF matrix towards UV irradiation; the growth kinetics of NPs in samples containing different amounts of precursor was studied. Morphological and chemical characterization revealed different size and distribution of the NPs in the different samples. The studied materials spin coated on planar gold electrodes devices were electrically tested showing a good R_{off} / R_{on} ratio and a relatively low switching voltage (3.2 V), thus demonstrating the applicability of the developed material in threshold switching devices.

References

1. Chua, L., Memristor-The missing circuit element. *IEEE Transactions on Circuit Theory* **1971,** *18* (5), 507-519.

2. Strukov, D. B.; Snider, G. S.; Stewart, D. R.; Williams, R. S., The missing memristor found. *Nature* **2008,** *453* (7191), 80-83.

3. Chua, L., Resistance Switching Memories Are Memristors. In *Memristor Networks*, Adamatzky, A.; Chua, L., Eds. Springer International Publishing: Cham, 2014; pp 21-51.

4. Kim, K.-H.; Gaba, S.; Wheeler, D.; Cruz-Albrecht, J. M.; Hussain, T.; Srinivasa, N.; Lu, W., A Functional Hybrid Memristor Crossbar-Array/CMOS System for Data Storage and Neuromorphic Applications. *Nano Letters* **2012,** *12* (1), 389-395.

5. Yang, J. J.; Strukov, D. B.; Stewart, D. R., Memristive devices for computing. *Nat Nano* **2013,** *8* (1), 13-24.

6. Borghetti, J.; Snider, G. S.; Kuekes, P. J.; Yang, J. J.; Stewart, D. R.; Williams, R. S., /`Memristive/' switches enable /`stateful/' logic operations via material implication. *Nature* **2010,** *464* (7290), 873-876.

7. Prezioso, M.; Riminucci, A.; Graziosi, P.; Bergenti, I.; Rakshit, R.; Cecchini, R.; Vianelli, A.; Borgatti, F.; Haag, N.; Willis, M.; Drew, A. J.; Gillin, W. P.; Dediu, V. A., A Single-Device Universal Logic Gate Based on a Magnetically Enhanced Memristor. *Advanced Materials* **2013,** *25* (4), 534-538.

8. Jo, S. H.; Chang, T.; Ebong, I.; Bhadviya, B. B.; Mazumder, P.; Lu, W., Nanoscale Memristor Device as Synapse in Neuromorphic Systems. *Nano Letters* **2010,** *10* (4), 1297-1301.

9. Sun, H.; Liu, Q.; Li, C.; Long, S.; Lv, H.; Bi, C.; Huo, Z.; Li, L.; Liu, M., Direct Observation of Conversion Between Threshold Switching and Memory Switching Induced by Conductive Filament Morphology. *Advanced Functional Materials* **2014,** *24* (36), 5679-5686.

10. Kyung Min Kim and Doo Seok Jeong and Cheol Seong, H., Nanofilamentary resistive switching in binary oxide system; a review on the present status and outlook. *Nanotechnology* **2011,** *22* (25), 254002.

11. Ella, G., TiO 2 -based memristors and ReRAM: materials, mechanisms and models (a review). *Semiconductor Science and Technology* **2014,** *29* (10), 104004.

12. Wang, J. C.; Hsu, C. H.; Ye, Y. R.; Lai, C. S.; Ai, C. F.; Tsai, W. F., High-Performance Multilevel Resistive Switching Gadolinium Oxide Memristors With Hydrogen Plasma Immersion Ion Implantation Treatment. *IEEE Electron Device Letters* **2014,** *35* (4), 452-454.

13. Yang, J. J.; Pickett, M. D.; Li, X.; OhlbergDouglas, A. A.; Stewart, D. R.; Williams, R. S., Memristive switching mechanism for metal//oxide//metal nanodevices. *Nat Nano* **2008,** *3* (7), 429-433.

14. Chiolerio, A.; Bocchini, S.; Crepaldi, M.; Bejtka, K.; Pirri, C. F., Bridging electrochemical and electron devices: fast resistive switching based on polyaniline from one pot synthesis using FeCl3 as oxidant and co-doping agent. *Synthetic Metals* **2017,** *229*, 72-81.

15. Chen, Y.; Liu, G.; Wang, C.; Zhang, W.; Li, R.-W.; Wang, L., Polymer memristor for information storage and neuromorphic applications. *Materials Horizons* **2014,** *1* (5), 489-506.

16. Tae-Wook Kim and Hyejung Choi and Seung-Hwan Oh and Minseok Jo and Gunuk Wang and Byungjin Cho and Dong-Yu Kim and Hyunsang Hwang and Takhee, L., Resistive switching characteristics of polymer non-volatile memory devices in a scalable via-hole structure. *Nanotechnology* **2009,** *20* (2), 025201.

17. Gao, S.; Song, C.; Chen, C.; Zeng, F.; Pan, F., Dynamic Processes of Resistive Switching in Metallic Filament-Based Organic Memory Devices. *The Journal of Physical Chemistry C* **2012,** *116* (33), 17955-17959.

18. Rajan, K.; Chiappone, A.; Perrone, D.; Bocchini, S.; Roppolo, I.; Bejtka, K.; Castellino, M.; Pirri, C. F.; Ricciardi, C.; Chiolerio, A., Ionic liquid-enhanced soft resistive switching devices. *RSC Advances* **2016,** *6* (96), 94128-94138.

19. Highly reproducible memory effect of organic multilevel resistive-switch device utilizing graphene oxide sheets/polyimide hybrid nanocomposite. *Applied Physics Letters* **2011,** *99* (4), 042108.

20. White, S. I.; Vora, P. M.; Kikkawa, J. M.; Winey, K. I., Resistive Switching in Bulk Silver Nanowire–Polystyrene Composites. *Advanced Functional Materials* **2011,** *21* (2), 233-240.

21. Tuning the electrical switching of polymer/fullerene nanocomposite thin film devices by control of morphology. *Applied Physics Letters* **2008,** *93* (20), 203309.

22. Rajan, K.; Bocchini, S.; Chiappone, A.; Roppolo, I.; Perrone, D.; Bejtka, K.; Ricciardi, C.; Pirri, C. F.; Chiolerio, A., Spin-coated silver nanocomposite resistive switching devices. *Microelectronic Engineering* **2017,** *168*, 27-31.

23. Midya, R.; Wang, Z.; Zhang, J.; Savel'ev, S. E.; Li, C.; Rao, M.; Jang, M. H.; Joshi, S.; Jiang, H.; Lin, P.; Norris, K.; Ge, N.; Wu, Q.; Barnell, M.; Li, Z.; Xin, H. L.; Williams, R. S.; Xia, Q.; Yang, J. J., Anatomy of Ag/Hafnia-Based Selectors with 1010 Nonlinearity. *Advanced Materials* **2017,** *29* (12), 1604457-n/a.

24. Song, J.; Woo, J.; Prakash, A.; Lee, D.; Hwang, H., Threshold Selector With High Selectivity and Steep Slope for Cross-Point Memory Array. *IEEE Electron Device Letters* **2015,** *36* (7), 681-683.

25. Kawahara, A.; Azuma, R.; Ikeda, Y.; Kawai, K.; Katoh, Y.; Hayakawa, Y.; Tsuji, K.; Yoneda, S.; Himeno, A.; Shimakawa, K.; Takagi, T.; Mikawa, T.; Aono, K., An 8 Mb Multi-Layered Cross-Point ReRAM Macro With 443 MB/s Write Throughput. *IEEE Journal of Solid-State Circuits* **2013,** *48* (1), 178-185.

26. Choi, B. J.; Zhang, J.; Norris, K.; Gibson, G.; Kim, K. M.; Jackson, W.; Zhang, M.-X. M.; Li, Z.; Yang, J. J.; Williams, R. S., Trilayer Tunnel Selectors for Memristor Memory Cells. *Advanced Materials* **2016,** *28* (2), 356-362.

27. Gibson, G. A.; Musunuru, S.; Zhang, J.; Vandenberghe, K.; Lee, J.; Hsieh, C.-C.; Jackson, W.; Jeon, Y.; Henze, D.; Li, Z.; Stanley Williams, R., An accurate locally active memristor model for S-type negative differential resistance in NbOx. *Applied Physics Letters* **2016,** *108* (2), 023505.

28. Roppolo, I.; Castellino, M.; Bejtka, K.; Rizza, G.; Perrone, D.; Coulon, P.-E.; Chiappone, A.; Rajan, K.; Bocchini, S.; Ricciardi, C.; Pirri, C. F.; Chiolerio, A., Resistive Switching in Polymer Nanocomposites by Matrix-Controlled in Situ Nanoparticles Generation. *The Journal of Physical Chemistry C* **2017,** *121* (26), 14285-14295.

29. Rajan, K.; Bocchini, S.; Chiappone, A.; Roppolo, I.; Perrone, D.; Castellino, M.; Bejtka, K.; Ricciardi, C.; Pirri, C. F.; Chiolerio, WORM and bipolar inkjet printed resistive switching devices based on silver nanocomposites. *Flexible and Printed Electronics* **2017,** *2* (2), 024002.

30. Chiolerio, A.; Chiappalone, M.; Ariano, P.; Bocchini, S., Coupling Resistive Switching Devices with Neurons: State of the Art and Perspectives. *Frontiers in Neuroscience* **2017,** *11*, 70.

31. Ramesh, G. V.; Porel, S.; Radhakrishnan, T. P., Polymer thin films embedded with in situ grown metal nanoparticles. *Chemical Society Reviews* **2009,** *38* (9), 2646-2656.

32. Roppolo, I.; Doriguzzi Bozzo, A.; Castellino, M.; Chiappone, A.; Perrone, D.; Bejtka, K.; Bocchini, S.; Sangermano, M.; Chiolerio, A., Dual step irradiation process for in situ generation and patterning of silver nanoparticles in a photocured film. *RSC Advances* **2016,** *6* (18), 14832-14843.

33. Nazar, R.; Ronchetti, S.; Roppolo, I.; Sangermano, M.; Bongiovanni, R. M., In Situ Synthesis of Polymer Embedded Silver Nanoparticles via Photopolymerization. *Macromolecular Materials and Engineering* **2015,** *300* (2), 226-233.

34. Guo, Q.; Ghadiri, R.; Weigel, T.; Aumann, A.; Gurevich, L. E.; Esen, C.; Medenbach, O.; Cheng, W.; Chichkov, B.; Ostendorf, A., Comparison of in Situ and ex Situ Methods for Synthesis of Two-Photon Polymerization Polymer Nanocomposites. *Polymers* **2014,** *6* (7).

35. Rajan, K.; Roppolo, I.; Bejtka, K.; Chiappone, A.; Bocchini, S.; Perrone, D.; Pirri, C. F.; Ricciardi, C.; Chiolerio, A., Performance comparison of hybrid resistive switching devices based on solution-processable nanocomposites. *Applied Surface Science* **2018,** *443*, 475-483.

36. Novara, C.; Petracca, F.; Virga, A.; Rivolo, P.; Ferrero, S.; Chiolerio, A.; Geobaldo, F.; Porro, S.; Giorgis, F., SERS active silver nanoparticles synthesized by inkjet printing on mesoporous silicon. *Nanoscale Research Letters* **2014,** *9* (1), 527.

37. Berthelot, T.; Le, X. T.; Jégou, P.; Viel, P.; Boizot, B.; Baudin, C.; Palacin, S., Photoactivated surface grafting from PVDF surfaces. *Applied Surface Science* **2011,** *257* (22), 9473-9479.

38. Švorčı; amp; x; k, V.; Ročková, K.; Ratajová, E.; Heitz, J.; Huber, N.; Bäuerle, D.; Bačáková, L.; Dvořánková, B.; Hnatowicz, V., Cell proliferation on UV-excimer lamp modified and grafted polytetrafluoroethylene. *Nuclear Instruments and Methods in Physics Research Section B: Beam Interactions with Materials and Atoms* **2004,** *217* (2), 307-313.

39. Xia, Y.; Xiong, Y.; Lim, B.; Skrabalak, S. E., Shape-Controlled Synthesis of Metal Nanocrystals: Simple Chemistry Meets Complex Physics? *Angewandte Chemie International Edition* **2009,** *48* (1), 60-103.

40. Mao, P.; Chen, J.; Xu, R.; Xie, G.; Liu, Y.; Gao, G.; Wu, S., Self-assembled silver nanoparticles: correlation between structural and surface plasmon resonance properties. *Applied Physics A* **2014,** *117* (3), 1067-1073.

41. Matsubayashi, A.; Fukunaga, K.; Tsuji, T.; Ataka, K.; Ohsaki, H., Multilayered Ordering of the Metal Nanoparticles in Polymer Thin Films under Photoirradiation. *Langmuir* **2011,** *27* (2), 733-740.

42. Matsubayashi, A.; Fukunaga, K.; Tanaka, K., Metal ions/ion clusters transport in glassy polymer films: construction of multi-layered polymer and metal composite films. *Journal of Materials Chemistry* **2012,** *22* (31), 15578-15585.

43. Deshmukh, R. D.; Composto, R. J., Surface Segregation and Formation of Silver Nanoparticles Created In situ in Poly(methyl Methacrylate) Films. *Chemistry of Materials* **2007,** *19* (4), 745-754.